Article:
Wei, M. S., Solodov, A. A., Pasley, J. et al. (2008) Study of relativistic electron beam production and transport in high-intensity laser interaction with a wire target by integrated LSP modeling. Physics of Plasmas. 083101. ISSN: 1089-7674

https://doi.org/10.1063/1.2965149

Study of relativistic electron beam production and transport in high-intensity laser interaction with a wire target by integrated LSP modeling

M. S. Wei,[1,a)] A. A. Solodov,[2] J. Pasley,[1,b)] R. B. Stephens,[3] D. R. Welch,[4] and F. N. Beg[1]
[1]*Center for Energy Research, University of California at San Diego, La Jolla, California 92093, USA*
[2]*Fusion Science Center and Laboratory for Laser Energetics, University of Rochester, Rochester, New York 14623, USA*
[3]*General Atomics, San Diego, California 92186, USA*
[4]*Voss Scientific LLC, Albuquerque, New Mexico 87108, USA*

(Received 12 March 2008; accepted 7 July 2008; published online 1 August 2008)

The results of a numerical study of high-intensity short-pulse laser interaction with wire targets are presented. Fast electron production and transport in solid density plasma is modeled using the implicit hybrid particle-in-cell code LSP [D. R. Welch *et al.*, Phys. Plasmas **13**, 063105 (2006)]. These simulations were performed with realistic target size and laser parameters and over times much longer than the laser pulse. Nonlinear interaction processes, i.e., microchanneling and density steepening, have been observed. The spectrum of the relativistic electrons produced has a reduced slope temperature compared to that predicted by ponderomotive scaling. Preformed underdense plasma has been found to bottleneck fast electrons due to the intense magnetic fields generated near the critical surface. In a thin long wire target, the overall propagation length of the fast electrons is about 160 μm; however, surface fields guide a small fraction of electrons to longer distances. These results are in good agreement with the experiments and have demonstrated that the modeling of electron transport relevant to fast ignition can be pursued in an integrated manner. © *2008 American Institute of Physics*. [DOI: 10.1063/1.2965149]

I. INTRODUCTION

In the reentrant cone guided fast ignition scheme,[1] energetic electrons produced in high-intensity short-pulse laser-plasma interaction (LPI) have to propagate through tens of micrometers of overdense plasma to ignite the precompressed core. Since this problem involves nonlinear laser-plasma interaction, the transport of a huge current ($\gg$MA) of fast electrons from the critical surface to the core, and an associated density change of many orders of magnitude, it presents astronomical computational challenges. Even with the state-of-the-art parallel supercomputers, full-scale three-dimensional (3D) fast ignition modeling is still beyond the current capabilities. A common practice is to examine individual components of the interaction with simplified models. Fast electron generation from the LPI in the critical density region, and their transport in the overdense region, are modeled separately using explicit particle-in-cell (PIC) methods and hybrid PIC methods, respectively. Standard explicit PIC modeling of LPI requires an extremely fine mesh [determined by consideration of the plasma Debye length, $\lambda_D(\mathrm{cm}) = 743 \times \sqrt{T/n}$, where T is in eV and n is in cm^{-3}. For example, $\lambda_D \sim 0.002$ μm for a plasma temperature $T = 100$ eV and a density of 10^{21} cm^{-3}] and small time steps ($c\Delta t < \Delta x/\sqrt{2}$, where Δx is the grid size). Otherwise numerical grid heating will occur and nonphysical results will be produced.[2] These factors limit the size of the plasma that can be incorporated in explicit PIC simulations, even on large parallel supercomputers. For a large-scale simulation of fast electron beam transport in overdense plasmas, implicit hybrid PIC methods, where the fast electrons are treated as particles and the dense background plasma as fluids, are commonly used. Such methods permit a much larger grid size and time step to be employed compared to that required in the explicit PIC method. In these hybrid PIC simulations, fast electrons with a distribution function obtained from the empirical scalings for slope temperature T_h, angular spread, and conversion efficiency at the given laser intensities are either injected into the cold dense fluid plasma or promoted from the cold background electrons. Such hybrid simulations have been very successful in modeling the fast electron beam transport in the solid or highly compressed plasma targets.[3–5] However, it should be noted that the above-mentioned electron transport modeling ignores relativistic electron re-interaction with the laser fields,[6] the effects of the laser plasma interaction caused density modification,[7] and the LPI produced intense fields near the interaction region[8] on the fast electron generation and propagation. In the regime relevant to fast ignition, substantially large preformed plasmas ($\sim$100s micrometers) are expected due to the interaction of the nanosecond long amplified spontaneous emission (ASE) pedestal of the main laser pulse (with an energy on the Joule level) with the target. Nonlinear plasma dynamics under the interaction of the high-intensity petawatt laser with such large preformed plasmas will significantly affect the fast

a)Electronic mail: mwei@ferp.ucsd.edu.
b)Present address: University of York, Heslington, York YO10 5DD, United Kingdom.

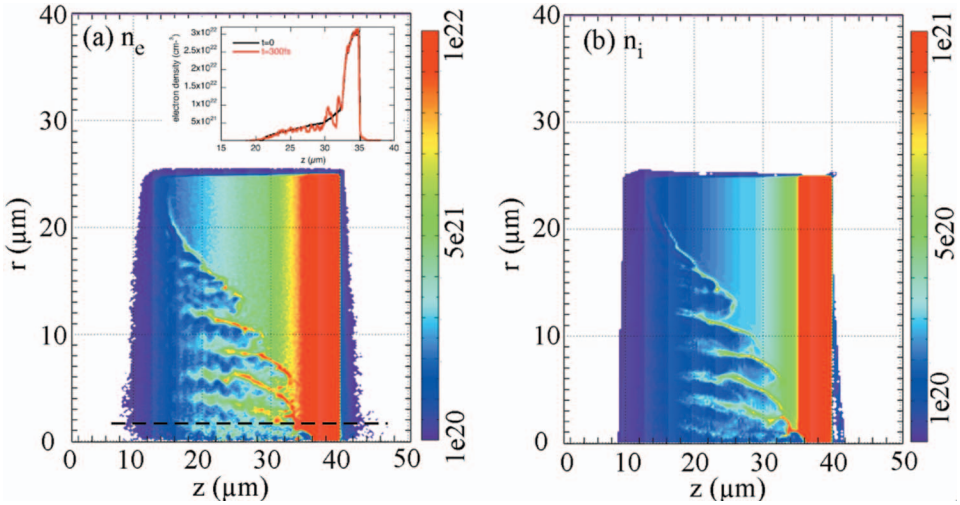

FIG. 1. (Color) Electron (a) and ion (b) density contour plots at 300 fs. Inset in (a) is the 1D electron density profile taking along the dashed line at $t=0$ and 300 fs. The laser was launched from the left boundary with a 0.5 ps pulse (square in time and Gaussian profile in the radial direction).

electron generation and must be taken into account in the predictive modeling of fast electron transport and target heating.

Recently, the hybrid implicit PIC code LSP[9–11] was used considerably in the modeling of laser-plasma interaction and fast ion acceleration from solid targets. The LSP code is a 3D electromagnetic PIC code designed for large-scale plasma simulations and uses an absolutely Courant-stable implicit method as the electromagnetic solver. Laser propagation in vacuum, its interaction with plasmas, and fast electron production can be included from first principles. Fully kinetic or dynamically re-allocated fluid/kinetic descriptions can incorporate a wide range of plasma densities. A novel direct-implicit scheme relaxes the usual PIC restrictions on the temporal and spatial resolutions and still maintains good energy conservation. Inter- and intraparticle interactions are determined by the Spitzer collision rate, and the ideal-gas model is used for the equation of state. In these newer LSP calculations, the interaction of hot electrons with the laser fields, physical effects from modified plasma densities, and hot electron interaction with the LPI induced strong fields are naturally included. To achieve this, a relatively finer grid size for the LPI interaction region is required (resulting in higher computational costs compared to the earlier LSP work reported in Refs. 3 and 4 where low-density preplasmas were ignored).

In this paper, we present integrated simulation results of fast electron transport in a wire target, using the hybrid implicit PIC code LSP, taken from a single simulation that includes the production of fast electrons from the laser plasma interaction. The small size wire target was employed specifically so as to enable simulations of the entire target to be performed, under realistic laser conditions, and over durations much longer than that of the laser pulse. We have found that the presence of preformed plasma significantly affects the fast electron generation and propagation. Fast electrons generated in the interaction of high-intensity laser with the included low-density preformed plasma have shown a two-temperature energy distribution. The high-energy component has a slope temperature comparable to the ponderomotive scaling, while the low-energy component has a reduced slope temperature of about 0.5–1 MeV. Preformed plasmas and the associated strong azimuthal magnetic fields have been found to bottleneck the fast electrons in the interaction region. We have also identified one of the main mechanisms for such strong magnetic field generation, i.e., the thermoelectric effect or the so-called $\nabla T \times \nabla n$ process. Fast electrons also have an overall propagation distance of ~ 160 μm in the wire target. In addition, a long-range surface current and resultant surface heating have also been observed. These results are in good agreement with our wire target experiments performed on the Titan laser at the Lawrence Livermore National Laboratory.[12] Our results have demonstrated the great importance of doing integrated simulation including a low-density performed plasma.

The paper is organized as follows: Implicit PIC simulation results of plasma dynamics and fast electron production are presented in Sec. II. In Sec. III, three key properties of the fast electron propagation, i.e., energy bottlenecking at the interaction region, overall limited propagation of fast electrons in the bulk of the target, and the surface heating, observed in the integrated simulation with the wire target are described. Conclusions are presented in Sec. IV.

II. SETUP AND RESULTS OF LSP MODELING OF THE LASER PLASMA INTERACTION

In LSP 3D cylindrical coordinates, the polarization and the phase of the laser electric field components are defined in Cartesian sense. This allows full control of the polarization—linear to circular. In our simulations, a linearly polarized (with only the E_x component) laser with 1 μm wavelength is launched from the left boundary propagating through a 20 μm vacuum region and interacting with 16 μm thick Ti plasmas with a 25 μm radius. The electron density of the pre-ionized Ti (15+) plasma increases from 10^{20} cm^{-3} to 3×10^{22} cm^{-3} in 13 μm thick steps and then stays constant for another 3 μm in the longitudinal direction [the density profile is shown in Fig. 1(a), inset]. The plasma density profile used is intended to mimic that created by the nanosecond long ASE prepulse of the main Titan laser.[13,14] For simplicity, the laser has a step profile in time (0.5 ps)

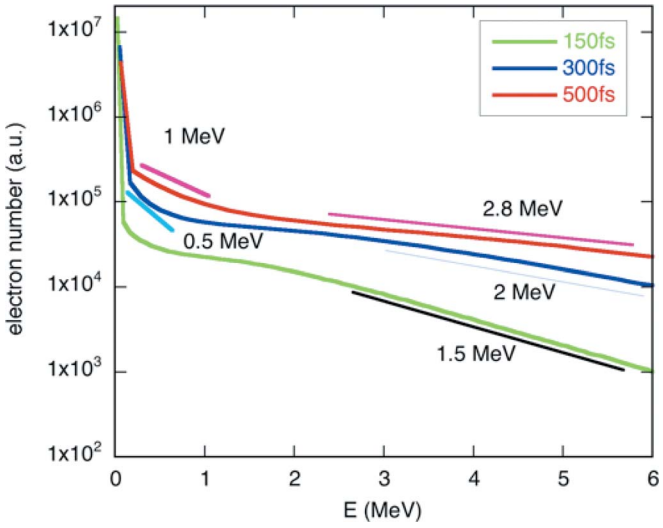

FIG. 2. (Color online) Energy spectra of the fast electrons produced by the high-intensity laser plasma interaction in LSP simulations.

with a peak intensity of 7.4×10^{19} W/cm^2 and a Gaussian profile in space (focal spot size of 15 μm). The simulation was performed in 3D cylindrical geometries ($R=40$ μm, $Z=60$ μm) with 2.38×10^6 cells. There are 36 particles per cell for both electron and ion species in the plasma region. Both species are treated kinetically. The grid size is 20 cells per laser wavelength and the time step $c\Delta t=0.03$ μm. The initial temperature of the plasma is set at 100 eV, which is much less than that used for the explicit PIC simulations (~keV temperatures). This initial temperature is chosen to cap the Spitzer resistance corresponding roughly to the actual resistance curve so that nonphysical high resistance at lower temperatures can be avoided.

Extremely nonlinear laser plasma interactions have been observed in the LSP simulation. Figure 1 shows the electron and ion density contour plots at 0.3 ps. The plasma electrons are pushed in both longitudinal and transverse directions by the laser ponderomotive force. At the laser propagation front, the electron density profile steepens with a density increase of about 2 as shown in the inset to Fig. 1(a). Microchannel formation is also observed in the intense laser region. These channels are first initiated in the underdense plasma region and then extend into the high-density plasma. The width of each individual channel is comparable to the laser wavelength (1 μm). The formation of these microchannels is likely due to the relativistic self-focusing and filamentation instabilities as the laser power is well above the threshold power for such instabilities to occur [$P_{\rm crit}=16.2(\omega_o/\omega_p)^2$ GW, where ω_p is the plasma frequency and ω_o is the laser frequency].[15] Such filamentation instability has also been observed in experiments with gas-jet generated underdense plasma. The width of the filaments is found to decrease with an increase of the plasma density to the laser wavelength.[16] These observed phenomena are consistent with simulations using collisionless explicit PIC codes.[17]

Figure 2 shows the energy spectrum of the fast electrons (>100 keV). The conversion efficiency from the laser to the fast electrons is about 53%. The fast electron spectrum can be fitted to a two-temperature Maxwellian distribution. The shape of the high-energy component evolves with time to a slope temperature of about 2.8 MeV, which is comparable to the laser ponderomotive energy. The spectrum of the lower-energy component evolves with time to about 1 MeV at the end of the laser pulse. The slope temperature for this lower-energy component is only about 1/3 of the ponderomotive energy. There is about 25% of the energy contained in the low-energy component and 75% in the high-energy component. It is noted that the lower-energy component only becomes noticeable after the microchanneling and density steepening (as seen in Fig. 1) occurred while the high-energy component exists from the beginning of the laser plasma interaction. This reduced slope temperature has also been observed in recent explicit PIC simulations by two other independent codes, OSIRIS[6] and PICLS,[7] and has been attributed to the steepening of the plasma density gradient, which simultaneously reduces the acceleration length available to the electrons. It is worth noting that predictions of reduced electron temperature have important implications for fast ignition, where hot electron energies must be limited to 1–3 MeV in order to heat the hot spot efficiently, but energy must be deposited with sufficient rapidity to overcome loss mechanisms, necessitating quite a high laser intensity. The angular distribution of the fast electron produced in the LSP simulation is almost isotropic.

The good agreement, in terms of plasma dynamics and fast electron generation, between the implicit LSP and other explicit collisionless or collisional PIC simulations, demonstrates that the LSP code can indeed be used for the integrated modeling of fast electron transport, including LPI. A detailed example of such modeling is described in the following section.

III. INTEGRATED LSP MODELING OF ELECTRON BEAM TRANSPORT IN THE WIRE TARGET

Integrated LSP simulations were performed to model the recent wire experiment carried out on the Titan laser at the Lawrence Livermore National Laboratory. The experimental results can be found in Ref. 12. One type of target used in the experiment was a 50 μm titanium wire with a length of ~700 μm. The laser was incident on the tip of the wire. In the integrated LSP simulations, the target is constructed as a region of preformed plasma, with a similar density profile to that shown above, followed by the Ti wire, which in the simulation is 400 μm in length (more than half of the length of the real target). It has a fixed ionization state of 15+ and an electron number density of 8.45×10^{23} cm^{-3} [1D electron number density profile $n(z)$ is shown in the inset to Fig. 3(b)]. Electrons are treated as kinetic particles in the preformed plasma region and as fluid species in the solid wire. They can transmute from one status to another according to their phase space, i.e., kinetic electrons with a directed energy less than 10 times the thermal temperature of the fluid electrons are converted back to fluid, and vice versa. Simulations were performed in 3D cylindrical geometries with 50 μm in R and 450 μm in Z. The linearly polarized laser, with the same peak intensity as that used in the previous

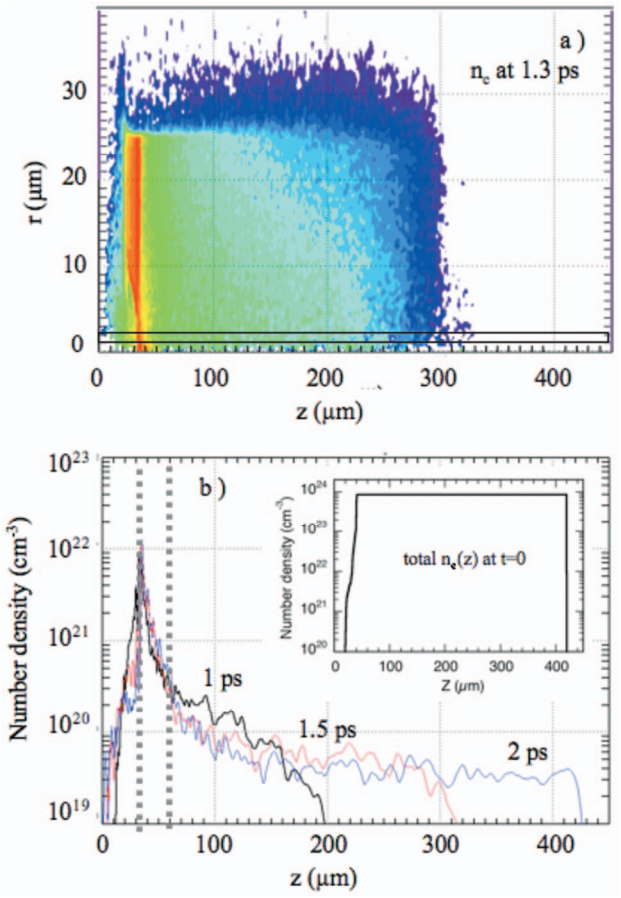

FIG. 3. (Color) (a) Fast electron density contour plot at 1.3 ps; (b) on-axis lineouts (r-cut, averaged over 1 μm thick width) of the fast electron number density. Inset in (b) is the initial on-axis electron (including both kinetic and fluid electrons) density profile used in the simulation. The time evolution of the fast electron propagation along the wire shows the bottlenecking of the fast electrons at the interaction region.

simulation, has a Gaussian profile in both time [0.4 ps full width at half-maximum (FWHM)] and space (9 μm focal spot size). To make a more efficient and practical simulation, the grid size is relatively larger than that used in the previous high-resolution simulations. In the preformed plasma region, $\Delta r=0.3$ μm, $\Delta z=0.18$ μm, and there are 45 particles per cell for both electrons and ions. In the solid target region, $\Delta r=0.6$ μm, $\Delta z=1$ μm, and there are 27 particles per cell. The initial temperature for both kinetic particles and the fluid is set at 100 eV. Simulations are performed using the IA-64 Linux cluster at the San Diego Supercomputer Center. Even with the reduced resolution, the code runs for 18 h on 32 nodes (dual processors) to reach 500 fs of simulation time. The total run to 3 ps takes about 108 h.

In this simulation with a reduced resolution, it is worth noting that although the microscopic phenomenon, i.e., microchanneling, cannot be really resolved anymore, the macroscopic features in plasma dynamic, i.e., density steepening with a bow-shaped contour as shown in Fig. 3(a), are maintained. Laser field penetrates into the critical density surface and is absorbed within a few laser wavelengths. About 60% of laser energy is transferred to fast electrons, which is comparable to that obtained in the high-resolution run (53%) shown in Sec. II. The fast electron energy spectrum also shows a two-temperature profile with the high-energy component having a slope temperature of ~2.8 MeV. The low-energy component now has a slightly lower slope temperature (~0.5 MeV). It should be noted that, similar to the high-resolution simulation results shown in Sec. II, the high-energy component is dominant due to the presence of the low-energy preformed plasmas in both simulations.

The most striking feature regarding the fast electron density profile is the drastic reduction of the number density along the wire axis. This can be seen clearly in Fig. 3(b), which shows lineouts [averaged over the 1 μm thick region indicated in (a)] of the fast electron number density at three different times after the laser pulse. In this plot, the kinetic electron number density decreases one order of magnitude in less than 25 μm inside the solid wire along the Z direction. This indicates that laser-produced fast electrons are bottlenecked near the interaction region. Phase-space data show that those electrons have a relatively low energy (<500 keV). Strong localized azimuthal magnetic fields, which extend from the critical surface to the lower density plasma region in a few-micrometer-thick layer, are observed both during the laser pulse (100 MG) and afterward (50 MG at 1.3 ps) and act to confine these electrons.

Such bottlenecking has been found to depend on the scale length of the preformed plasma that obscures the solid target. Figure 4 shows fast electron number density and magnetic fields from two LSP simulations that were performed for comparison, in which all of the other parameters are identical, except for the preformed plasma condition. One simulation includes preformed plasma, the other does not. Fast electrons with an isotropic Maxwellian distribution in phase space were promoted at the 3X relativistic corrected critical surface in a 1 μm thick layer from the background plasma using the ponderomotive scaling for a given laser intensity (5×10^{19} W/cm^2). These simulations, using the excitation model for fast electron generation (this method has been successfully established and used in previous work[3–5]), were performed to examine the effects of the preformed plasma on the fast electron propagation. To well resolve the low-density preplasma and reduce the numerical noise, a fine mesh size (with a minimum value of 0.25 μm) and a large number of particles (170) per cell were used for the preplasma region. Such simulations have a high computational cost that is comparable to that in the integrated LSP simulations. It took about 4 days to reach 1 ps of the simulation time with 10 processors. We have found that with a preformed plasma, more electrons remain near the critical surface region. The fast electron number density at the critical surface region with the preformed plasma case is more than four times greater than that with the steep density case as shown in Figs. 4(a)–4(d). It should be noted that the electrons that are confined have energies less than 500 keV. Examining the fields [see Figs. 4(e) and 4(f)] in these two cases suggests that intense localized azimuthal magnetic fields (~50 MG) just outside the critical surface, in the low density plasma region, play an important role in trapping those less energetic electrons and inhibiting their propagation into the solid target. These fields are generated due to the hot electrons, which go from the

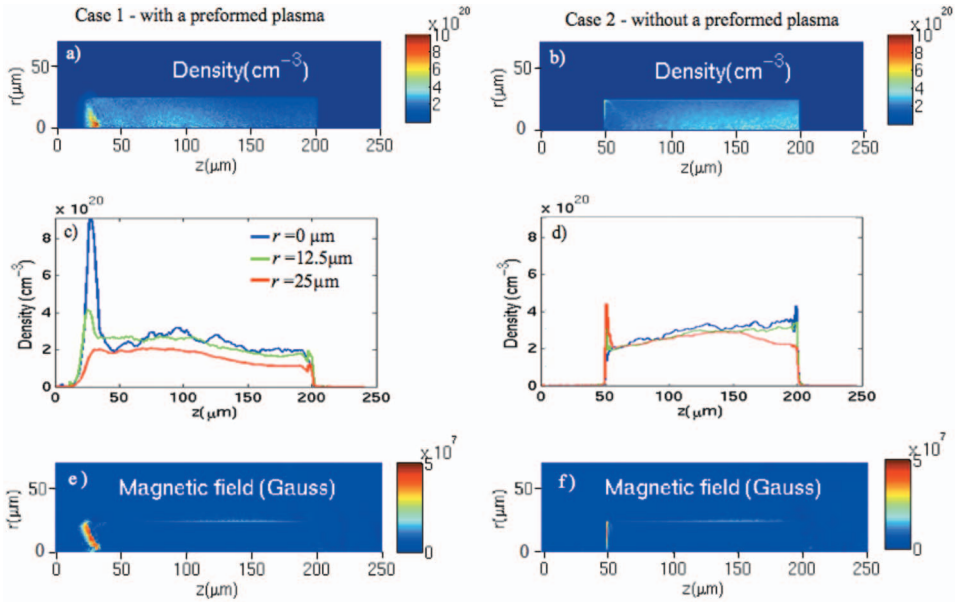

FIG. 4. (Color) Fast electron density contour (a) and (b), lineouts (r-cut) (c) and (d), and the azimuthal magnetic fields (e) and (f) for two different preformed plasma conditions. (a), (c), and (e) are with a preformed plasma $n=n_0\exp(-0.28\times|z-|)$, $z<z_0$, $z_0=50$ μm; and (b), (d), and (f) are for the steep density condition without a preformed plasma. For this figure only, the simulations used a 0.5 ps laser pulse with a square profile in time and a Gaussian profile in the radial direction. The intensity on-axis was 5×10^{19} W/cm^2. The hot electrons were promoted from plasma electrons with the mean energy found from the ponderomotive scaling for a local laser intensity. The plots are shown 0.5 ps after the laser pulse.

dense plasma into a low density region or vacuum in the steep density case. Near the critical surface, the counter effects of the E field (due to the charge separation) and the B fields confine more electrons at the critical surface. Those trapped electrons are also found to laterally propagate along the surface of the target. The trapped electrons are responsible for the density maximum in the region of the strong magnetic field. In the preformed plasma case, due to the presence of the extended region of the low density plasma, more energetic electrons go out into the low density plasma region as compared to the case in which there is no preformed plasma. The magnetic field can exist in a much thicker layer of the plasma compared to the steep density gradient case (note that B fields with a similar magnitude are also present in the steep density gradient case, but only extend through a less than 1 μm thick surface layer). Therefore, the inhibition of electron transport due to magnetic field trapping becomes more pronounced when there exists a long scale length preformed plasma. Similar surface magnetic fields were observed in the simulations at much lower laser intensities using CO_2 lasers[18] and were attributed to the thermoelectric effect or the so-called $\nabla T\times\nabla n$ process. At the front target surface, the net electron component has a density gradient in the longitudinal direction and an average temperature gradient in the radial direction. So, the electric field $E\sim-\nabla P/en$ (with $P=nkT$) has a nonzero curl and generates an azimuthal magnetic field according to Faraday's law. For the parameters used in the simulation with $\nabla n/n=2.8\times10^3$/cm, $\nabla T\times\nabla n$ gives a field B(MG)$\sim140\times T$[MeV]. The maximum B field at 0.5 ps in the simulation is about 80 MG This corresponds to an estimated plasma temperature of about 0.570 MeV, which is certainly of the same order as the T_h (1.1 MeV) used in the simulations. At high laser intensities, as in the present simulation, the hot electron behavior also resembles a fountain in which electrons leaving the irradiated spot toward the vacuum return to the target at the margins of the spot. The surface magnetic fields and electron trapping were also observed in the hybrid simulations of Mason.[5]

Following the initial drastic reduction in number density, the fast electron profile [$n(z)$ versus z] further into the solid target has a much slower decay. This is also confirmed in the fast electron current profile shown in Fig. 5. The 1/e length of this smooth decay gives an overall propagation distance of ~160 μm, which is slightly shorter than that observed by the $K\alpha$ luminescent emission measurements in the experiment (~200 μm). This difference may be due to the limited simulation time (~3 ps, only about 1/3 of the original hot electron energy has thermalized by this time) compared to the long lifetime of the MeV electrons. Recent experiments have suggested that $K\alpha$ emission lasts longer than 10 ps at high intensities ($>10^{19}$ W/cm^2).[19] The limited fast electron propagation distance is mainly attributed to the bulk Ohmic inhibition of the fast electrons proposed by Bell *et al.*[20] With

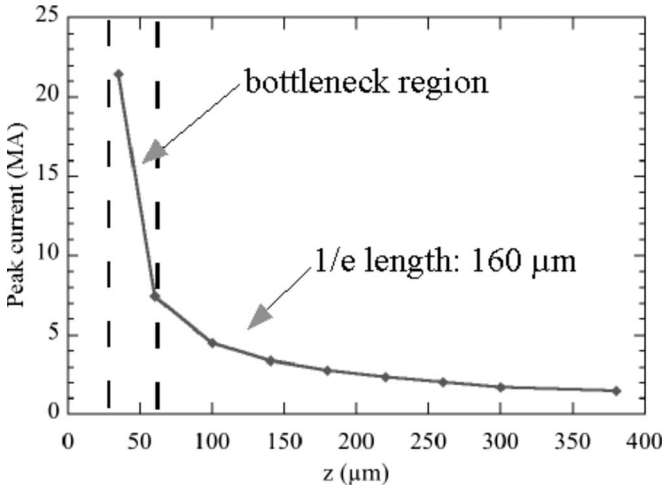

FIG. 5. Fast electron peak current along the z direction showing both the bottlenecking and an overall propagation length (1/e) of 160 μm.

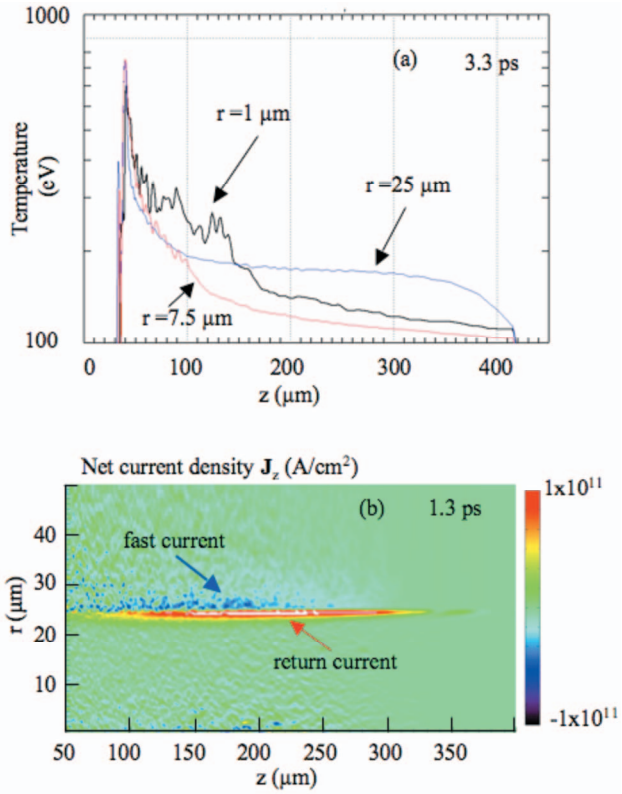

FIG. 6. (Color) (a) Background electron temperature lineouts at three different radii showing a higher temperature on the surface, and (b) net current density contour plot suggesting a localized return current on the surface that results in the surface heating.

the given laser intensity and the known conductivity of the Ti plasma at 100 eV ($\sim 1.4\times 10^6\ \Omega^{-1}\ m^{-1}$), Bell's model predicts a propagation distance $\sim 120\ \mu$m, which is similar to that observed in our simulations and in the experiments. LSP simulations with a lower initial temperature (10 eV, which gives unphysical high resistance) show a shorter propagation distance. Our results also agree with recent e-PLAS results where both magnetic inhibition (taking place near the critical surface region) and resistive inhibition (on the $\sim 100\ \mu$m scale) were identified.[21]

In addition to the transport in the bulk of the target, LSP simulations also show long-range surface transport and the resultant surface heating. Figure 6(a) shows the lineout of the background plasma electron temperatures at 3.3 ps. Beyond $\sim 100\ \mu$m from the interaction region along the wire axis direction, the wire surface was heated more than that inside (180 eV on the surface versus 120 eV inside). The slope of the decay is almost flat at greater distances from the interaction region. On the wire surface, intense azimuthal B-fields ($\sim$40 MG) and radial electric fields ($\sim$MV/μm) have also been observed. The formation of such surface fields and surface current transport and heating have been proposed and investigated previously by various authors.[22,23] Fast electrons coming to the transverse boundary at an angle leave the wire and move outside until they are turned back by the transverse sheath field. Therefore, there is a longitudinal current of fast electrons outside the wire that creates a magnetic field. The surface current of plasma electrons [as shown in Fig. 6(b), net current density plot] develops to shield and prevent the field penetration into the plasma. The return current in the shield layer heats up the plasma and leads to the observed higher surface temperature. It should be noted that in our simulations, this surface current is only a very small fraction of the total current as it extends only to about a 1 μm thin layer (resolution limited). The ratio of the surface current to the total current is proportional to the ratio of the thickness of this layer to the wire radius. In our simulations, this ratio is less than 4%. The observed long-range surface current and heating agree qualitatively with the experiments where surface plasma thermal emissions and the $K\alpha$ fluorescence were observed out to distances of $\sim$1 mm in some cases.

IV. CONCLUSIONS

High-intensity short-pulse relativistic laser-plasma interaction, fast electron production, and transport in a solid target have been modeled using the implicit hybrid PIC code LSP. All the important macroscopic nonlinear physics have been well reproduced in the LSP simulation with relaxed constraints on the temporal and spatial requirements as compared to conventional explicit PIC methods. Comparing our results with those from explicit PIC codes, we have observed similar energy conversion efficiency from the laser to fast electrons as well as the reduced slope temperature in the electron spectrum. This consistency check has demonstrated that LSP modeling is a practical integrated solution for the study of laser-produced fast electron transport and heating in solid targets.

The integrated simulations for the wire target have revealed important physics governing fast electron transport. We have observed the bottlenecking of fast electrons at the critical surface region, where the plasma density has been significantly modified by the huge (Gbar) laser pressure. This retention of fast electrons at the interaction surface is caused by the local intense magnetic fields. The effects of the preformed plasma on the magnetic inhibition of fast electron transport have been examined and are in agreement with e-PLAS hybrid PIC simulation results.[5] Magnetic field trapping of electrons with energies of less than 500 keV at the interaction surface may account for the observed peak $K\alpha$ fluorescence at the target front surface due to the large cross section of $K\alpha$ production for the electrons trapped or stopped there. Our results are also consistent with the recent fully PIC simulations, using the PICLS code, where stronger magnetic fields were observed at the critical surface region in the longer preformed plasma condition, resulting in reduced coupling to the solid target.[24] Our findings may have significant importance for fast ignition as a better energy coupling may be achievable by controlling the scale length of the preformed plasma as suggested by the LSP simulations. This will be further investigated using the integrated LSP simulation.

The overall limited propagation distance, caused by the Ohmic inhibition of the fast electron transport in the solid wire target, in the integrated LSP simulations, is in reasonable agreement with the experiments. Simulations have also confirmed the existence of long-range surface current (guided by the surface E and B fields) and the resultant surface heating

by the return current as is observed in the experiment. Though it is similar to that suggested in the explicit PIC simulations, it should be noted that we have found that the amount of the current and the degree of heating are sensitive to the density and temperature of the plasma. More work is required to quantify this surface phenomenon for better comparison with the experiment.

ACKNOWLEDGMENTS

This work was performed under the auspices of the U.S. Department of Energy under Contract Nos. DE-FC02-04ER54789 (Fusion Science Center), DE-FG02-05ER54834, and DE-FG03-00ER54606. This work is also partially supported by the National Center for Supercomputing Applications under Grant Nos. TG-PHY050034T, TG-PHY060020T, and TG-PHY070008T.

[1] R. Kodama, P. A. Norreys, Y. Sentoku, and R. B. Campbell, Fusion Sci. Technol. **49**, 316 (2006), and references therein.
[2] C. K. Birdsall and A. B. Langdon, *Plasma Physics Via Computer Simulation* (Institute of Physics, London, 2005).
[3] R. P. J. Town, C. Chen, L. A. Cottrill, M. H. Key, W. L. Kruer, A. B. Langdon, B. F. Lasinski, R. A. Snavely, C. H. Still, M. Tabak, D. R. Welch, and S. C. Wilk, Nucl. Instrum. Methods Phys. Res. A **554**, 61 (2005); R. P. J. Town, L. A. Cottrill, M. H. Key, W. L. Kruer, A. B. Langdon, B. F. Lasinski, B. C. McCandless, J. F. Myatt, H. S. Park, B. A. Remington, R. A. Snavely, C. H. Still, M. Tabak, D. R. Welch, and S. C. Wilks, U.S. DOE Office for Science and Technical Information (www.osti.gov), No. 881057 (2006).
[4] R. B. Campbell, J. S. DeGroot, T. A. Mehlhorn, D. R. Welch, and B. V. Oliver, Phys. Plasmas **10**, 4169 (2003); R. B. Campbell, R. Kodama, T. A. Mehlhor, K. A. Tanaka, and D. R. Welch, Phys. Rev. Lett. **94**, 055001 (2005).
[5] R. J. Mason, and C. Cranfill, IEEE Trans. Plasma Sci. **PS-14**, 45 (1986); R. J. Mason, E. S. Dodd, and B. J. Albright, Phys. Rev. E **72**, 015401(R) (2005); R. J. Mason, Phys. Rev. Lett. **96**, 035001 (2006).
[6] J. Tonge and W. Morri (private communication).
[7] B. Chrisman, Y. Sentoku, and A. J. Kemp, Phys. Plasmas **15**, 056309 (2008).
[8] M. Tatarakis, I. Watts, F. N. Beg, E. L. Clark, A. E. Dangor, A. Gopal, M. G. Haines, P. A. Norreys, U. Wagner, M.-S. Wei, M. Zepf, and K. Krushelnick, Nature (London) **415**, 280 (2002); U. Wagner, M. Tatarakis, A. Gopal, F. N. Beg, E. L. Clark, A. E. Dangor, R. G. Evans, M. G. Haines, S. P. D. Mangles, P. A. Norreys, M.-S. Wei, M. Zepf, and K. Krushelnick, Phys. Rev. E **70**, 026401 (2004).
[9] D. R. Welch, D. V. Rose, M. E. Cuneo, R. B. Campbell, and T. A. Mehlhorn, Phys. Plasmas **13**, 063105 (2006).
[10] R. G. Evans, High Energy Density Phys. **2**, 355 (2006).
[11] T. P. Hughes, S. S. Yu, and R. E. Clark, Phys. Rev. ST Accel. Beams **2**, 110401 (1999); D. R. Welch, D. V. Rose, B. V. Oliver, and R. E. Clark, Nucl. Instrum. Methods Phys. Res. A **464**, 134 (2001).
[12] J. Pasley, M. Wei, E. Shipton, S. Chen, T. Ma, F. N. Beg, N. Alexander, R. Stephens, A. G. MacPhee, D. Hey, S. Le Pape, P. Patel, A. Mackinnon, M. Key, D. Offermann, A. Link, E. Chowdhury, L. Van-Woerkom, and R. R. Freeman, Phys. Plasmas **14**, 120701 (2007).
[13] P. Patel (private communication).
[14] J. Pasley (private communication).
[15] G. Sun, E. Ott, Y. C. Lee, and P. Guzdar, Phys. Fluids **30**, 526 (1987).
[16] A. G. R. Thomas, Z. Najmudin, S. P. D. Mangles, C. D. Murphy, A. E. Dangor, C. Kamperidis, K. L. Lancaster, W. B. Mori, P. A. Norreys, W. Rozmus, and K. Krushelnick, Phys. Rev. Lett. **98**, 095004 (2007).
[17] Y. Sentoku, W. Kruer, M. Matsuoka, and A. Pukhov, Fusion Sci. Technol. **49**, 278 (2006), and references therein.
[18] D. W. Forslund and J. U. Brackbill, Phys. Rev. Lett. **48**, 1614 (1982).
[19] H. Chen, R. Shepherd, H. K. Chung, A. Kemp, S. B. Hansen, S. C. Wilks, Y. Ping, K. Widmann, K. B. Fournier, G. Dyer, A. Faenov, T. Pikuz, and P. Beiersdorfer, Phys. Rev. E **76**, 056402 (2007).
[20] A. R. Bell, J. R. Davies, S. Guerin, and H. Ruhl, Plasma Phys. Controlled Fusion **39**, 653 (1997).
[21] R. J. Mason, R. B. Stepens, M. Wei, R. R. Freeman, J. Hill, and L. D. Van Woerkom, "Short pulse laser driven relativistic electron transport in wire targets," presented at the 9th International Fast Ignition Workshop, Cambridge, MA (2006).
[22] R. Kodama, Y. Sentoku, Z. L. Chen, G. R. Kumar, S. P. Hatchett, Y. Toyama, T. E. Cowan, R. R. Freeman, J. Fuchs, Y. Izawa, M. H. Key, Y. Kitagawa, K. Kondo, T. Matsuoka, H. Nakamura, M. Nakatsutsumi, P. A. Norreys, T. Norimatsu, R. A. Snavely, R. B. Stephens, M. Tampo, K. A. Tanaka, and T. Yabuuchi, Nature (London) **432**, 003133 (2004); Y. Sentoku, K. Mima, H. Ruhl, Y. Toyama, and R. Kodama, Phys. Plasmas **11**, 3083 (2004); T. Nakamura, S. Kato, H. Nagatomo, and K. Mima, Phys. Rev. Lett. **93**, 265002 (2004).
[23] J. S. Green, K. L. Lancaster, K. U. Akli, C. D. Gregory, F. N. Beg, S. N. Chen, D. Clark, R. R. Freeman, S. Hawkes, C. Hernandez-Gomez, H. Habara, R. Heathcote, D. S. Hey, K. Highbarger, M. H. Key, R. Kodama, K. Krushelnick, I. Musgrave, H. Nakamura, M. Nakatsutsumi, N. Patel, R. Stephens, M. Storm, M. Tampo, W. Theobald, L. Van Woerkom, R. L. Weber, M. S. Wei, N. C. Woolsey, and P. A. Norreys, Nat. Phys. **3**, 853 (2007).
[24] Y. Sentoku (private communication).